# High coke resistance of a $TiO_2$ Anatase (001) catalyst surface during dry reforming of methane

THE JOURNAL OF PHYSICAL CHEMISTRY C



C: Surfaces, Interfaces, Porous Materials, and Catalysis

# The High Coke Resistance of a TiO Anatase (001) Catalyst Surface during Dry Reforming of Methane

Stijn Huygh, Annemie Bogaerts, Kristof M. Bal, and Erik Cornelis Neyts

*J. Phys. Chem. C*, **Just Accepted Manuscript** • DOI: 10.1021/acs.jpcc.7b10963 • Publication Date (Web): 17 Apr 2018

# The High Coke Resistance of a $TiO_2$ Anatase (001) Catalyst Surface during Dry Reforming of Methane

Stijn Huygh, Annemie Bogaerts, Kristof M. Bal, Erik C. Neyts*

Research Group PLASMANT, Department of Chemistry, University of Antwerp, Universiteitsplein 1, B-2610 Antwerp, Belgium

*Corresponding author:

Tel: +32-3-265.23.88

Fax: +32-3-265.23.43

e-mail: erik.neyts@uantwerpen.be

## Abstract

The resistance of a $TiO_2$ anatase (001) surface to coke formation was studied in the context of dry reforming of methane using Density Functional Theory (DFT) calculations. As carbon atoms act as precursors for coke formation, the resistance to coke formation can be measured by the carbon coverage of the surface. This is related to the stability of different $CH_x$ (x = 0 – 3) species and their rate of hydrogenation and dehydrogenation on the $TiO_2$ surface. Therefore, we studied the reaction mechanisms and their corresponding rates as function of the temperature for the dehydrogenation of the species on the surface. We found that the stabilities of C and CH are significantly lower than those of $CH_3$ and $CH_2$. The hydrogenation rates of the different species are significantly higher than the dehydrogenation rates in a temperature range of 300 – 1000 K. Furthermore, we found that dehydrogenation of $CH_3$, $CH_2$ and CH will only occur at appreciable rates starting from 600, 900 and 900 K, respectively. Based on these results, it is clear that the anatase (001) surface has a high coke resistance, and it

is thus not likely that the surface will become poisoned by coke during dry reforming of methane. As the rate limiting step in dry reforming is the dissociative adsorption of $CH_4$, we studied an alternative approach to thermal catalysis. We found that the temperature threshold for dry reforming is at least 700 K. This threshold temperature may be lowered by the use of plasma-catalysis, where the appreciable rates of adsorption of plasma-generated $CH_x$ radicals result in bypassing the rate limiting step of the reaction.

# 1 Introduction

The anthropogenic increase of the greenhouse effect by the emission of greenhouse gases has led to changes in the global climate.[1–4] NASA reports that nine of the warmest years in the last 136 years occurred post the year 2000, and the 10$^{th}$ warmest year is 1998.[5] From all greenhouse gases $CO_2$ and $CH_4$ contribute the most to the anthropogenic greenhouse effect.[6] The average global tropospheric $CO_2$ concentration has increased from 280 ppm in 1750[7] to 404 ppm in December 2016[8], and the average global tropospheric $CH_4$ concentration has increased from 722 ppb in 1750[7] to 1844 ppb in September 2016[8]. The major challenge in fighting the global climate change is the decrease of the greenhouse gas concentrations, while the global population keeps growing and the global economy keeps developing.

Several mitigation strategies exist to decrease the greenhouse gas concentrations. The most obvious strategy is the reduction of the emission itself. However, it will be necessary to combine this strategy with the conversion of $CO_2$ and $CH_4$ to value-added chemicals, as this will result in a strong decrease in greenhouse gas concentrations and reduce our dependence on fossil fuels. Dry reforming of methane is a highly attractive process from an environmental point of view as one uses waste gases to form chemical feedstock. Indeed, the combination of $CO_2$ and $CH_4$ allows the use of low-grade natural gas that is obtained as by-product at oil platforms, which is otherwise flared, or one can use biogas as a renewable feedstock for the chemical industry. In dry reforming of methane, $CO_2$ is used to oxidize $CH_4$ to syngas, i.e., a mixture of CO and $H_2$:

$$CH_4 + CO_2 \rightarrow 2CO + 2H_2 \qquad \Delta H^o_{298} = 59\ kcal.mol^{-1}$$

Syngas can then be utilized for the chemical synthesis of fuels, e.g. through the Fischer-Tropsch synthesis.[9] Furthermore, oxygenated products such as methanol, ethanol and

aldehydes can be synthesized from syngas.[10] Other uses of syngas are its direct combustion[11], and the use of the water gas shift reaction to increase the $H_2$ content and use the hydrogen in the Haber-Bosch process to generate ammonia. However, it would also be beneficial to directly form value-added chemicals, apart from syngas, through dry reforming of methane.

The most popular catalysts for dry reforming are nickel-based catalysts.[12–16] The main problem for commercialisation of dry reforming is that these catalysts are prone to coke formation.[13,17,18] Wang et al. reported that the coke formation probability is inversely related to the dominance of the CH oxidation pathway over the CH reduction pathway.[13] These pathways are in turn dependent on the relative stability of the different $CH_x$ species and the relative rates of hydrogenation and dehydrogenation of the $CH_x$ species. Based on the tendency of nickel-based catalysts to be poisoned by the formation of coke, it is necessary to study different materials with respect to their resistance to coke formation. In this contribution we report on the hydrogenation and dehydrogenation reactions of different adsorbed $CH_x$ ($x = 0 - 3$) species on a titanium dioxide anatase (001) surface, as studied using Density Functional Theory (DFT) calculations. Based on the results presented in this paper, it is evident that the anatase surface has a high coke resistance, and will thus not be prone to deactivation by coke formation on the surface. In thermal catalytic dry reforming of methane $TiO_2$ is not used as catalyst, but rather as support for catalytic metal particles. It is reported to increase the coking-resistance of the catalyst.[19–23] However, it is reported that the presence of $TiO_2$ is important for the catalytic activity of the catalyst, e.g. neither pure Pt nor pure $TiO_2$ shows appreciable conversions for dry reforming of methane.[19] The activity of the $Pt/TiO_2$ catalyst is assigned to the activation and conversion of $CO_2$ on the $TiO_2$ support by adsorption on a Lewis base center, while the methane is activated on the metal surface[24] forming $CH_x$ and H species.

The available $CH_x$ species adsorbed on the surface will play an important role in the dry reforming of methane. Indeed, in our previous studies we demonstrated that the adsorption and the reduction of $CO_2$ greatly depends on the availability of oxygen vacancies in the anatase (001) surface.[25] The reduction of $CO_2$ is found to be impossible on the defect-free surface, while oxygen vacancies significantly reduce the energy barrier, and can result in exothermic dissociation of $CO_2$. However, during the reduction of $CO_2$ the oxygen vacancies are healed, and thus a regeneration mechanism is required

to continue the $CO_2$ reduction. The $CH_x$ species adsorbed on the surface will act as reductants, and can form oxygenated products such as formaldehyde, methanol and CO, depending on the reaction rates and on the availability of the different $CH_x$ species on the surface.

Furthermore, due to the high endothermicity and energy barriers of dry reforming, high temperatures and a catalyst are required to obtain significant conversions of $CH_4$ and $CO_2$ at an acceptable rate. Other challenges than the high energy requirement relate to the state of the catalyst, including sintering, sulphur poisoning, coke formation and maintaining a sufficiently high activity.[26] It is therefore opportune to pursue alternative technologies. A combination of a non-thermal atmospheric plasma with a catalyst, i.e., plasma-catalysis, is a promising technique, since the plasma will activate the gas mixture, inducing reactions at lower temperatures, while the catalyst can reduce the activation barriers and increase the selectivity.[27] Due to the high complexity of the plasma-catalytic system, the exact mechanisms are far from understood.[28–30] Wei et al. reported that the rate limiting step in both dry and steam reforming of methane on nickel is the dissociative adsorption of $CH_4$.[31] Previously, we also studied the adsorption of methane derived radicals, formed in a plasma,[32,33] and the effect of oxygen vacancies on the adsorption.[34] Here, we study the effect of the use of plasma-catalysis on the temperature threshold of dry reforming on an anatase (001) surface using DFT calculations. The combination of a plasma with $TiO_2$ allows the activation of methane in the plasma discharge, generating $CH_x$ and H radicals which will adsorb and react on the $TiO_2$ surface.[32,35] Note that under real conditions is is likely that the $TiO_2$ surface is partially covered by OH groups, as water is known to dissociatively adsorb on the (001) facet. The results presented in this work give thus insight in the reaction mechanisms of plasma-catalysis on pristine $TiO_2$. Furthermore, the results form an initial step for a study of the dry reforming of methane on a $TiO_2$ supported metal catalyst.

In the next sections we address whether or not $TiO_2$ is prone to coke formation, which can deactivate the surface, and how the temperature dependence of the dry reforming of methane changes by comparing thermal and plasma catalysis.

## 2 Computational details

All calculations are performed at the DFT-GGA level using the Vienna ab initio simulation package (VASP).[36,37] For the treatment of the exchange and correlation, the Perdew-

Burke-Ernzerhof (PBE) functional was applied,[38] using plane wave basis sets and the projector-augmented wave method[39] as implemented in VASP. We have corrected the PBE functional with long-range dispersion interactions by applying the Tkatchenko and Scheffler method[40] as implemented in VASP.[41] The stoichiometric anatase (001) surface was modelled using a (2x2) supercell containing 48 atoms corresponding to four $TiO_2$ layers. We fixed the bottom layer of the surface at the bulk positions and the simulation box was created to maintain a vacuum layer of ~16 Å between adjacent surfaces to prevent the influence of neighbouring slabs on the calculated energies and reactions. The sampling of the Brillouin zone was performed using a 6x6x1 k-points grid for the surface models whereas only the gamma-point was taken into account for the molecules and the radicals. An energy cut-off of 440 eV was used. Geometry optimizations were performed with the conjugate gradient method, with the endpoint criterion for the residual forces set to 0.03 $eV.Å^{-1}$. Spin polarization was applied for all calculations.

Since $TiO_2$ is a strongly correlated metal-oxide, standard GGA typically fails to describe the electronic structure, and in particular the electronic structure of defect states. This can be resolved either by applying hybrid functionals (which are, however, very time consuming in comparison to GGA) or by employing the DFT+U approach. For the latter, however, the results tend to be very dependent on the specific choice of the U-parameter. Therefore, to keep the results transparent and feasible, we have chosen to employ the GGA-approach.

Note that the most stable anatase $TiO_2$ surface is the (101) facet. We have here chosen to model the (001) surface instead, as this significantly reduces the computational effort required to obtain initial insight in the surface reactions on the anatase surfaces, while still providing the fundamental information this study aims at. The root cause for this major difference in computational effort is the number of $TiO_2$ layers required for convergence, which is higher for the anatase (101) surface than for the (001) surface. Furthermore, due the high symmetry of the (001) surface, the possible adsorption configurations are significantly reduced compared to (101), further reducing the computational cost.

For the same reason, we have chosen to model the unreconstructed surface, instead of, e.g., the (001) 1x4 reconstruction. Note however, that oxygen stabilizes the unreconstructed surface, and in the dry reforming reaction $CO_2$ will act as an oxygen source such that the unreconstructed surface is stabilized during the reaction.

As mentioned above, the unreconstructed (001) anatase surface may contain OH surface groups, possibly affecting the reaction pathways. We here focus solely on the accessible pathways on the pure $TiO_2$ surface, in order to limit the number of possible reactions and adsorption configurations.

Vibrational analysis was performed with the finite difference method implemented in VASP. The calculations included the displacements to both the adsorbed molecules and the top layer of the $TiO_2$ surface. These results were used for the thermodynamical analysis, as performed with the TAMKIN tool.[42] All reported energies are corrected for the zero-point energy. TAMKIN was used for the determination of the Gibbs Free Energy and reaction rate constants applying Transition State Theory. To determine resistance to coke formation and the available $CH_x$ species, we calculated the corresponding dehydrogenation minimal energy pathways (MEP) with Nudged Elastic Band (NEB)[43–48].

The colour code for the different elements of the configurations shown in all figures below is as follows: Ti = light gray, O = red, H = white, C = dark gray. In all reported energy values, negative values for •H and •G indicate exothermic and exergonic processes, respectively, and positive values for •H and •G indicate endothermic and endergonic processes, respectively. Below, we report the half-lives of the calculated reactions; the conversion from the half-lives, $t_{1/2}$, to the reaction rate constants, k, can be done as follows:

$$k_i = \frac{\ln 2}{t_{\frac{1}{2},i}}$$

In the case of the non-activated adsorption of the radicals, we have calculated the rate constant using kinetic gas theory. The half-life of non-activated adsorption on a specific adsorption site is calculated as follows:

$$t_{\frac{1}{2},ads} = \frac{\ln 2}{\sqrt{\frac{k_b\, T}{2\pi M}} * A * C}$$

where $M$ is the mass of the gas-phase species, A the surface area of one adsorption site and C the concentration of the gas phase species as based on the results of Snoeckx et al.[32].

For the desorption linked to the non-activated adsorption, the rate constant is calculated using the following equation[49]:

$$k_{des} = \frac{k_b * T}{h} * \exp\left(-\left(\frac{G_{gas} + G_{surf} - G_{ads} + S_{1D-trans} * T}{R * T}\right)\right)$$

where $G_{gas}$, $G_{surf}$, $G_{ads}$, and $S_{1D\text{-}trans}$ correspond to the Gibbs free energy of the gas-phase species, the surface left behind after desorption, and the adsorbed configuration, and the entropy contribution of the translational degree of freedom perpendicular to the surface, respectively. Thus the transition state corresponds to the system in the state where the desorbed molecule is far away from the surface, i.e., when the molecule no longer interacts with the surface. The entropy of this transition state is identical to that of the gas-phase radical, except for the entropy contribution of the translational degree of freedom perpendicular to the surface that is removed.

# 3 Results and discussion

## 3.1. $CH_x$ (x = 1 – 3) dehydrogenation: Thermodynamics

As starting geometries for the dehydrogenation reactions of the different $CH_x$ species (x = 1 – 3), we took the most stable adsorption configurations as reported in our previous work.[34] The configurations and reaction products after dehydrogenation are shown in Figure 1. After dehydrogenation of $CH_3$ and $CH_2$ the hydrogen is either bonded to the 2-coordinated oxygen, $O_{2c}$, or to the first subsurface 3-coordinated oxygen, $O_{3c}$ (see Figure 1). For the CH dehydrogenation only the $O_{3c}$ configuration is found to be stable. The reaction enthalpy is corrected for the zero-point energy. All reactions are found to be endothermic, as indicated in the figure.

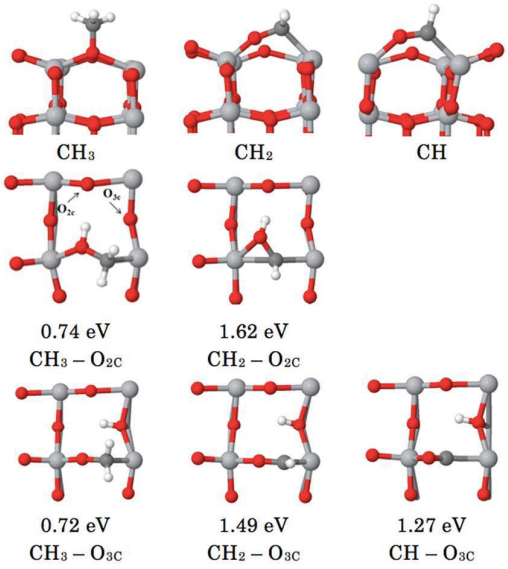


**Figure 1. Side view of the most stable adsorption configurations of the $CH_x$ species (x = 1 – 3) (top-row), and top-view of the reaction products after dehydrogenation. The second row corresponds to reaction products where H is bonded to $O_{2c}$, while the third row corresponds to H bonded to $O_{3c}$. The reaction enthalpies are given below each configuration. In the first structure of the second row we indicate a two-coordinated oxygen $O_{2c}$, and a three-coordinated $O_{3c}$.**

In Figure 2 the Gibbs free energy of reaction is given for the different dehydrogenation reactions at temperatures ranging from absolute zero to 1000 K. All reactions are found to be endergonic at all considered temperatures, and thus the equilibrium will lie towards the hydrogenated reactants. The temperature only exerts a small influence on the relative stabilities between the reactants and reaction products, with a maximum difference of -0.1 eV between absolute zero and 1000 K for $CH_3 – O_{XC}$.

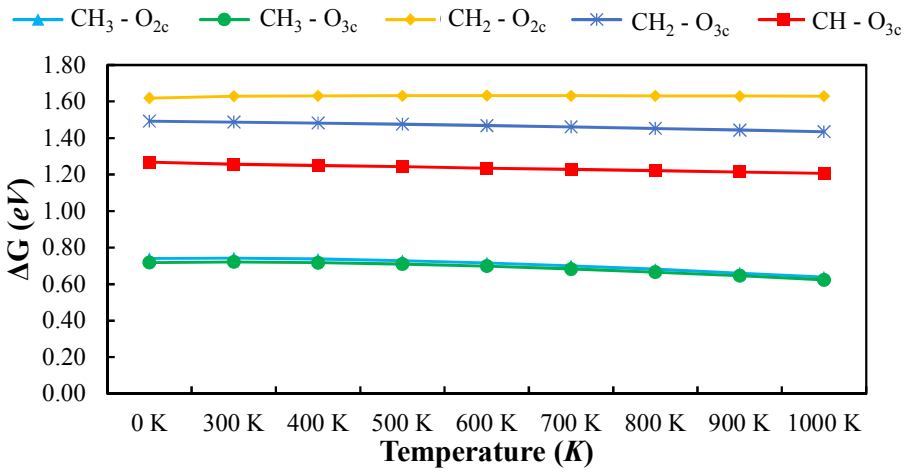


**Figure 2. Gibbs free energy of reaction for dehydrogenation of the $CH_x$ species (x = 1-3) with hydrogen either adsorbed at the $O_{2c}$ atom bonded to the $CH_{x-1}$ radical or to the $O_{3c}$ site neighbouring the reaction site. (see Figure 1)**

However, if the reaction products, i.e. $CH_{x-1}$ and H, further separate and move to their individually preferred sites through hydrogen diffusion, the relative stability of the dehydrogenated radical increases compared to the radical, as is shown in Figure 3. In this case there is no distinction between the binding site of H, as it will be bonded in its most stable configuration, i.e., bonded to the $O_{2c}$ atom. The relative stability of the $O_{2c}$ and $O_{3c}$ binding sites for the H atom is -0.67 eV, coinciding with the value found by Hussain et al.[50] The increased stability of the end products results in an exergonic reaction for the $CH_3$ dehydrogenation, from a reaction free energy of 0.10 eV at absolute zero to -0.29 eV at 1000 K. $CH_2$ and CH dehydrogenation remain endergonic, even when the reaction products are separated.

The overall dehydrogenation reaction can also be made more favourable if it results in the formation and desorption of hydrogen gas. However, as is the case for the separation of the reaction products to their preferred binding sites, the dehydrogenation of $CH_2$ and CH remain endergonic over the entire considered temperature range (see Figure 3). On the other hand, for the dehydrogenation of $CH_3$ the reaction becomes exergonic between 500 and 600 K. Thus both the desorption, and the product separation results in a shift of the equilibrium towards $CH_2$. (see Figure 3)

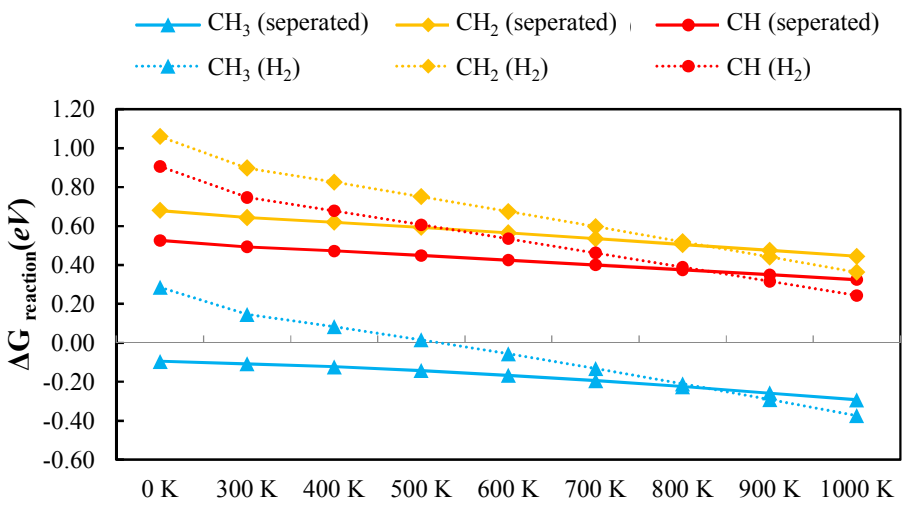


**Figure 3. Relative stability of the $CH_x$ radical with his dehydrogenated counterpart $CH_{x-1}$ + H after product separation (solid lines) and with his dehydrogenated counterpart $CH_{x-1}$ + 0.5 $H_2$ (dotted lines).**

## 3.2. Hydrogen diffusion

We have determined the minimal energy pathway for the hydrogen diffusion, between the $O_{2c}$ binding site and the $O_{3c}$ binding site, as shown in Figure 4. The entire diffusion pathway connecting the most stable sites consists of a consecutive diffusion from $O_{2c}$ to $O_{3c}$ followed by diffusion from $O_{3c}$ to $O_{2c}$. Thus in Figure 4 only half the pathway is shown, the total pathway is symmetric over the $O_{3c}$ configuration (final state in Figure 4). Both reaction steps are taken into account for the half-lives given in Figure 4. At elevated temperatures, hydrogen diffusion occurs rapidly. For instance, at 600 K the half-life equals 4.5 μs. As the hydrogen can diffuse rapidly over the surface, it is possible to have both $CH_3$ and $CH_2$ species to be present on the surface, as the equilibrium of the dehydrogenation reaction of $CH_3$ can be pushed to $CH_2$ by the removal of the resulting H-atom, either by diffusion or by reaction of hydrogen to form one of the end-products of dry reforming. Based on the thermodynamics, i.e., the higher relative stability of $CH_3$ and $CH_2$ versus CH and C, both the $CH_3$ and $CH_2$ species will be readily available on the surface for other reactions to occur, while CH and C will become hydrogenated and will not play a significant role in the reactions. In the next section we will show that also the kinetics of the process corroborates this interpretation.

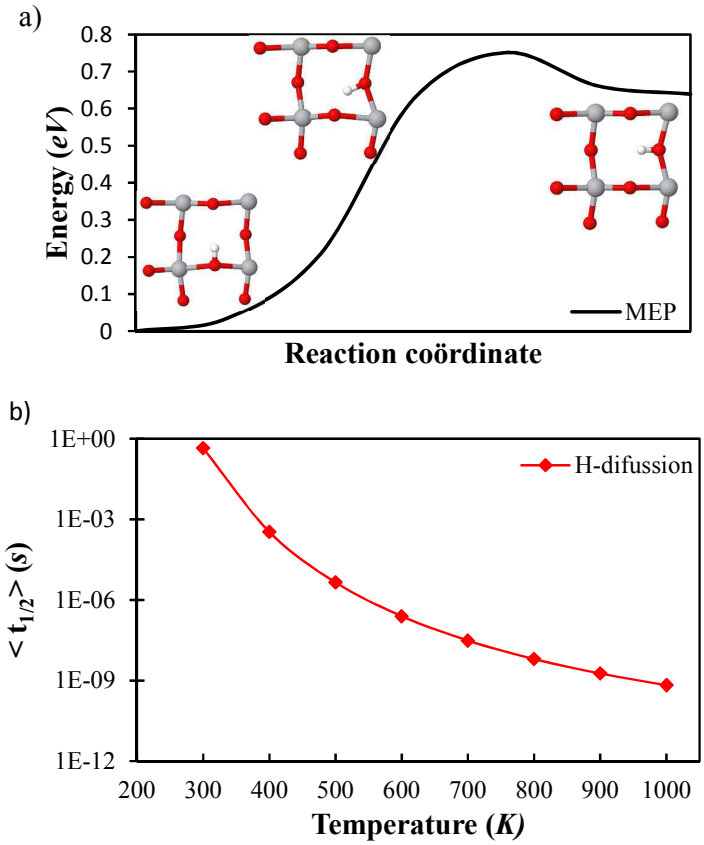


**Figure 4. a) Minimal energy pathway (MEP) for H-diffusion $O_{2c}$ to $O_{3c}$ and b) half-life for the H-diffusion to occur.**

## 3.3. $CH_x$ (x = 1 – 3) dehydrogenation: Kinetics

### 3.3.1. $CH_3$ dehydrogenation

In Figure 5 the minimal energy pathways and half-lives for the dehydrogenation of $CH_3$ and the hydrogenation of $CH_2$ is given with the abstracted H bonded to $O_{2c}$ and $O_{3c}$. The energy barrier for the dehydrogenation is significantly lower when the abstracted hydrogen is bonded to the $O_{3c}$ compared to when it is bonded to the $O_{2c}$. The barriers for dehydrogenation are 1.26 eV and 2.94 eV, respectively. The high barrier for the $O_{2c}$ route will prevent the dehydrogenation from occurring at an appreciable rate even at 1000 K, where the half-life for the reaction is equal to 0.47 s. Instead, dehydrogenation through the $O_{3c}$ pathway will proceed at elevated temperatures. The hydrogenation is always faster than the dehydrogenation, but this will be partially counteracted by the diffusion of hydrogen away from the reaction site. The energy gain by the diffusion of hydrogen

results in the end product of dehydrogenation to be more stable than the $CH_3$ radical, as shown above.

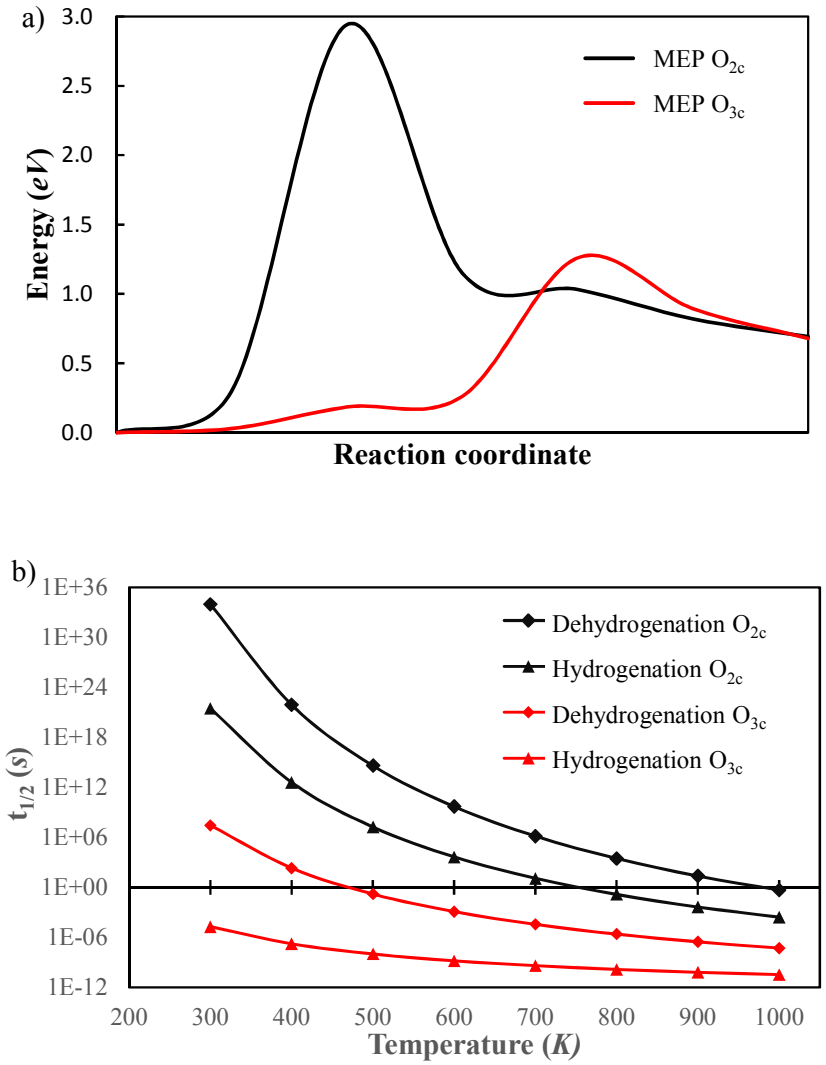


**Figure 5. a) Minimal energy pathway (MEP) as calculated with NEB for the dehydrogenation of $CH_3$, and b) the half-life for the hydrogenation of $CH_2$ and the dehydrogenation $CH_3$.**

In Figure 6 the minimal energy pathways and half-lives for the dehydrogenation of $CH_2$ and the hydrogenation of CH are given with the abstracted H bonded to $O_{2c}$ and $O_{3c}$. Also in the case of $CH_2$ we find that the $O_{3c}$ route is the more viable route compared to the $O_{2c}$ route. However, the reaction rate for the dehydrogenation of $CH_2$, even at elevated temperatures, is significantly lower than for the dehydrogenation of $CH_3$, e.g. at 600 K the half-life is $4x10^4$ times greater than for the $CH_2$ dehydrogenation, and at 1000 K it is

700 times greater. Similar to $CH_3$, the hydrogenation reaction of $CH_2$ is significantly faster than the dehydrogenation. When hydrogen diffuses away from the reaction site to stabilize the reaction products, we find that $CH_2$ stays significantly more stable than the dehydrogenated products, thus indicating that the dehydrogenation reaction will halt at the $CH_2$ radical.

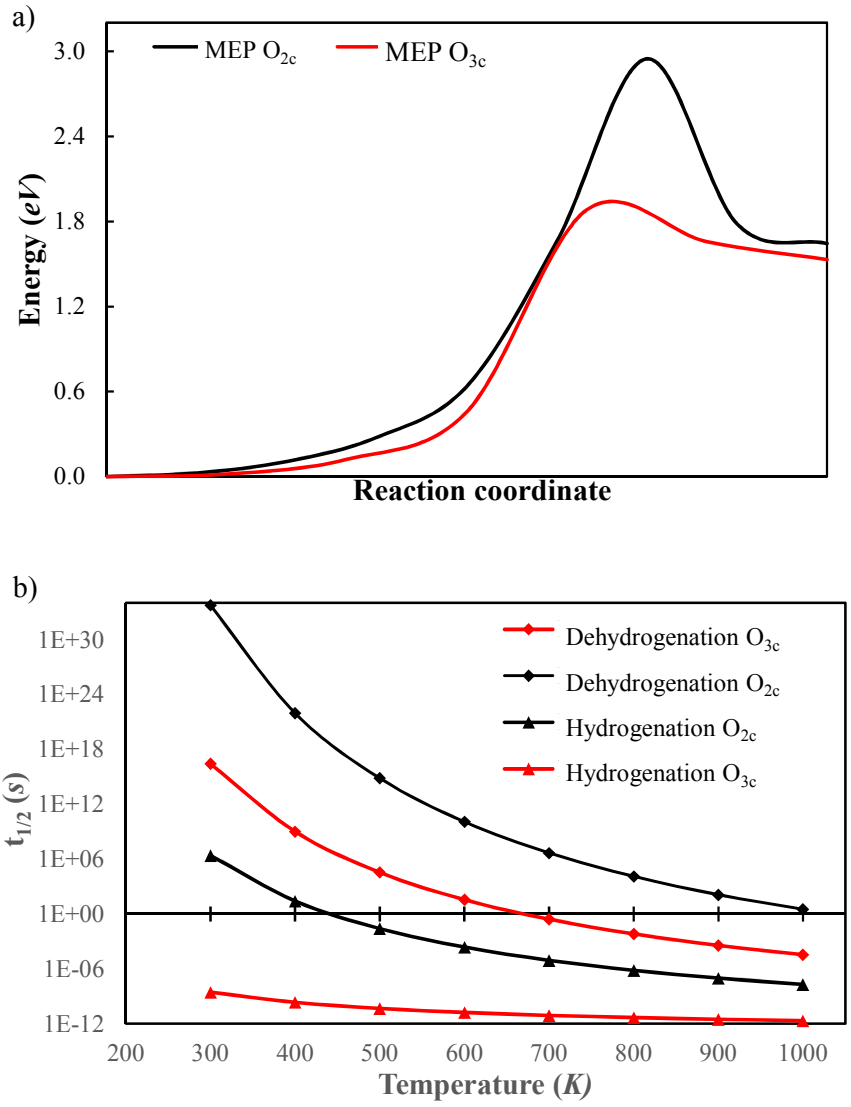


**Figure 6. a) Minimal energy pathway (MEP) as calculated with NEB for the dehydrogenation of $CH_2$, and b) the half-life for the hydrogenation and dehydrogenation reactions.**

### 3.3.2. CH dehydrogenation

In Figure 7 the minimal energy pathways and half-lives for the dehydrogenation of CH and the hydrogenation of C are given. For CH the dehydrogenation can only result in the abstracted hydrogen to end up at $O_{3c}$, as the configuration with H bonded to $O_{2c}$ is found to be unstable. The reaction rate of the dehydrogenation and hydrogenation of CH is very similar to that of $CH_2$. Also in this case we find that the hydrogenation is significantly faster than the dehydrogenation reaction. As for $CH_2$ dehydrogenation, the diffusion of H to a more stable adsorption site will not result in a higher stability of the reaction products, i.e., C and H, compared to the CH radical.

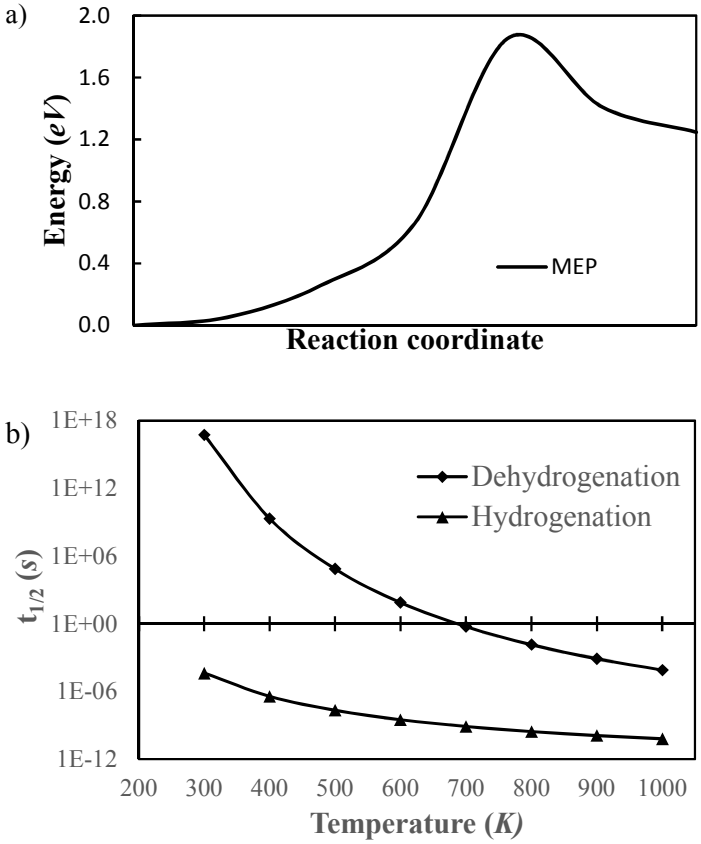


**Figure 7. a) Minimal energy pathway (MEP) as calculated with NEB for the dehydrogenation of CH with hydrogen bonded to $O_{3c}$, and b) the half-life for the hydrogenation and dehydrogenation reactions.**

The probability of coke formation on a catalyst surface is dependent on the coverage of the surface by carbon atoms[13], as these carbon atoms are found to be the precursors for coke.[51,52] Due to the low stability of both CH and C on the surface, and the low ratio in

dehydrogenation-to-hydrogenation rates of the $CH_x$ species, we can conclude that anatase (001) exhibits no tendency to become poisoned by coke formation.

## 3.4. Plasma-catalysis

We also studied the influence of the use of plasma-catalysis on the rate-determining step of thermal catalytic dry reforming of methane, i.e., the dissociative adsorption of $CH_4$ on the catalyst surface. The dissociative adsorption of $CH_4$ is an endothermic process, for which the adsorption energy on anatase (001) is equal to 0.48 eV. The corresponding activation barrier is equal to 0.77 eV. In Figure 8 it is seen that the temperature must exceed 900 K before the half-life of dissociative adsorption of $CH_4$ drops below 1 ms. An appreciable rate of adsorption will only be obtained at temperatures of 700 – 900 K, while the half-life of adsorption is equal to ~$10^{-12}$ s for the considered temperature range (300 – 1000 K). The temperature threshold for the dry reforming reaction can be lowered by removing the rate limiting step in the reaction. In plasma-catalytic dry reforming of methane this is accomplished by electron impact dissociation of $CH_4$ to different $CH_x$ radicals in the plasma phase. [32,33]

In Figure 8 we show the average waiting time for the adsorption of $CH_x$ (x = 0 – 3) and H per unit cell, based on the average densities of these species as calculated by Snoeckx et al.[32], and the average waiting time for desorption of these species on both the hydrogenated and the clean surface, all in a temperature range of 300 – 1000 K. We only show the cases for which the half-life of reaction is lower than 1000 s. Thus, the C and CH desorption are not shown, as the half-life of desorption in the considered temperature range is always larger than 1000 s. The influence of the temperature on the rates of adsorption, and thus on the half-life of adsorption, is negligible for all species, compared to the temperature influence on desorption, as $k_{ads}$ depends on the square root of the temperature, while $k_{des}$ depends on the temperature as follows ~ T.exp(-1/T). This causes the desorption of $CH_3$ on both the clean and the hydrogenated surface to become faster than the adsorption above 500 K, and the desorption of $CH_2$ on the hydrogenated surface will only be observed significantly above 800 K and on the clean surface will only be observed above the considered temperature range. Hydrogen desorption as a radical will occur through the adsorption configuration with the hydrogen on the $O_{3c}$ site, as the combination of hydrogen diffusion with desorption is faster than the direct desorption of H from the $O_{2c}$ site. At 700 K, the

average waiting time of desorption will be around the ms range, and it becomes faster than adsorption above 800 K. As can be seen from the average waiting time for the different species to adsorb on a unit cell, the adsorption of C and CH are slower than $10^{-2}$ s, while the adsorption of $CH_2$, $CH_3$, and H are faster than 0.1 ms. Thus these latter species will be readily available on the surface. Especially $CH_3$ and H will be present all over the surface, and can diffuse easily starting from 500 K and 400 K (see Figure 4), respectively. We approximate the diffusion of $CH_3$ by assuming desorption and readsorption on the surface.

The adsorption of $CH_3$, $CH_2$ and H is significantly faster at all temperatures than the dissociative adsorption of $CH_4$, and their half-life of adsorption is lower than 1 ms in the considered temperature range. Therefore, we can conclude that the plasma-catalytic dry reforming results in a lower temperature threshold for the dry reforming of methane than in thermal reforming.

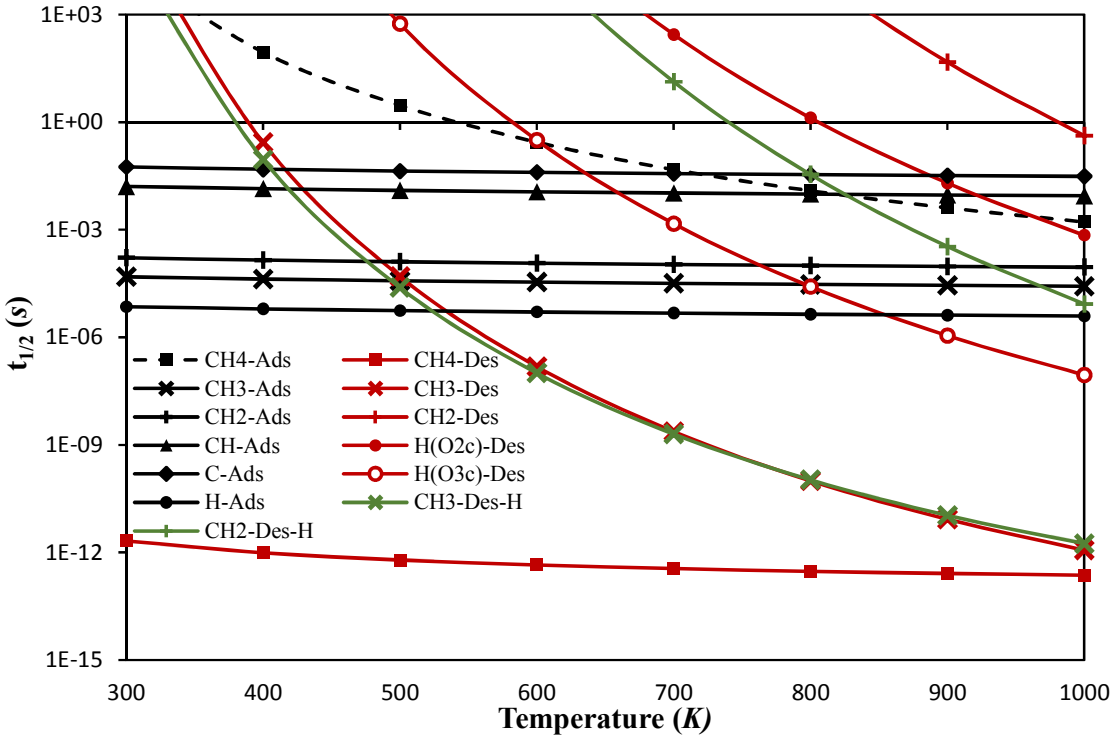

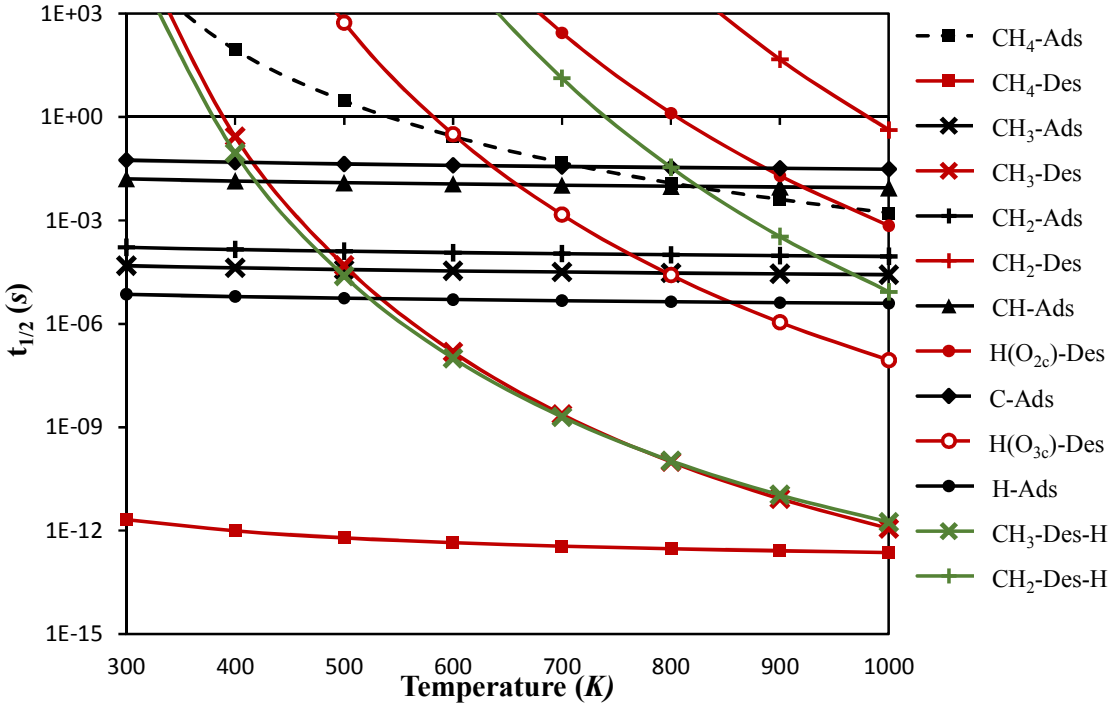


**Figure 8. Half-lives of adsorption (X-Ads, black), and desorption on the clean (X-Des, red) and hydrogenated (X-Des-H, green) surface for $CH_3$, $CH_2$, CH, C and H.**

## 4 Conclusion

We have studied the tendency of a pristine anatase (001) surface to become poisoned by coke formation during dry reforming of methane into value-added chemicals. For this purpose we applied DFT calculations with the PBE exchange-correlation functional with long range dispersion energy corrections of Tkatchenko and Scheffler[40]. To enable a direct comparison with experiments, certain important aspects would additionally need to be addressed in the calculations, including the presence of OH-groups on the surface, the relative stabilities of the (001) and (101) surfaces and the possible surface reconstruction of the (001) facet.

The readily available methane derived radicals are $CH_3$, $CH_2$, and H, since further dehydrogenation is thermodynamically and kinetically limited. The stability of CH and C is limited, and the hydrogenation of the different $CH_x$ is found to have appreciable rates over the complete temperature range of 300 – 1000 K, while the half-lives for the dehydrogenation are found only to be lower than 1 ms at 600, 900 and 900 K for $CH_3$,

$CH_2$ and CH, respectively. This will result in a low carbon coverage during dry reforming on the anatase (001) surface, which is advantageous as carbon would act as precursor for coke formation.

We found that the rate limiting step in dry reforming of methane, i.e., the dissociative adsorption of $CH_4$, results in a temperature threshold of 700 – 900 K. However, in plasma-catalytic dry reforming, this step can be circumvented by the adsorption of plasma generated $CH_x$ and H radicals, for which the half-life of adsorption of $CH_3$, $CH_2$ and H will be below 1 ms over the complete temperature range, 300 – 1000 K. Thus, by means of plasma-catalysis the temperature threshold can be lowered, and the overall reaction will be determined by the rate of the surface reactions.

## 5 Acknowledgments

The authors gratefully acknowledge financial support from the Fund for Scientific Research – Flanders (FWO; grant no: G.0217.14N), the TOP research project of the Research Fund of the University of Antwerp (grant ID: 32249) and the IAP/7 (Inter-university Attraction Pole) program 'PSI-Physical Chemistry of Plasma-Surface Interactions' by the Belgian Federal Office for Science Policy (BELSPO). The computational resources and services used in this work were provided by the VSC (Flemish Supercomputer Center), funded by the Research Foundation - Flanders (FWO) and the Flemish Government – department EWI.

## 6 References

(1) Pachauri, R. K.; Meyer, L. A. *IPCC, 2014: Climate Change 2014: Synthesis Report. Contribution of Working Groups I, II and III to the Fifth Assessment Report of the Intergovernmental Panel on Climate Change; IPCC, Geneva, Switzerland, 2014.*

(2) Pachauri, R. K.; Reisinger, A. *IPCC, 2014: Climate Change 2007: Synthesis Report. Contribution of Working Groups I, II and III to the Fourth Assessment Report of the Intergovernmental Panel on Climate Change; IPCC, Geneva, Switzerland, 2007.*

(3) Oreskes, N. The Scientific Consensus on Climate Change. *Science.* **2005**, *306*, 2004–2005.

(4) Balzani, V.; Credi, A.; Venturi, M. Photochemical Conversion of Solar Energy. *ChemSusChem*. **2008**, *1*, 26–58.

(5) NASA. Climate Change: Vital Signs of the Planet: Global Temperature. http://climate.nasa.gov/vital-signs/global-temperature/ (Date accesed: May 31, 2016)

(6) Indarto, A.; Choi, J. W.; Lee, H.; Song, H. K. Decomposition of Greenhouse Gases by Plasma. *Environ. Chem. Letters* **2008**, *6*, 215–222.

(7) [Stocker, T.F.; Qin, D.; Plattner, G.-K.; Tignor, M.; Allen, S. K.; Boschung, J.; Nauels, A.; Xia, Y. ; Bex, V.; Midgley, P.M. 2*013: Summary for Policymakers. In: Climate Change 2013: The Physical Science Basis. Contribution of Working Group I to the Fifth Assessment Report of the Intergovernmental Panel on Climate Change; Cambridge University Press,* Cambridge, United Kingdom and New York, NY, USA. 2013.

(8) ESRL Global Monitoring Division, Global Greenhouse Gas Reference Network. https://www.esrl.noaa.gov/gmd/ccgg/trends/ (Date accesed: December 14, 2016)

(9) Dry, M. E. The Fischer-Tropsch Process: 1950-2000. *Catal. Today* **2002**, *71*, 227–241.

(10) Subramani, V.; Gangwal, S. K. A Review of Recent Literature to Search for an Efficient Catalytic Process for the Conversion of Syngas to Ethanol. *Energy Fuels*. **2008**, *22*, 814–839.

(11) Lee, M. C.; Seo, S. Bin; Chung, J. H.; Kim, S. M.; Joo, Y. J.; Ahn, D. H. Gas Turbine Combustion Performance Test of Hydrogen and Carbon Monoxide Synthetic Gas. *Fuel* **2010**, *89*, 1485–1491.

(12) Zhu, Y. A.; Chen, D.; Zhou, X. G.; Yuan, W. K. DFT Studies of Dry Reforming of Methane on Ni Catalyst. *Catal. Today* **2009**, *148*, 260–267.

(13) Wang, Z.; Cao, X. M.; Zhu, J.; Hu, P. Activity and Coke Formation of Nickel and Nickel Carbide in Dry Reforming: A Deactivation Scheme from Density Functional Theory. *J. Catal.* **2014**, *311*, 469–480.

(14) Lv, X.; Chen, J. F.; Tan, Y.; Zhang, Y. A Highly Dispersed Nickel Supported Catalyst for Dry Reforming of Methane. *Catal. Commun.* **2012**, *20*, 6–11.

(15) Tsyganok, A. I.; Tsunoda, T.; Hamakawa, S.; Suzuki, K.; Takehira, K.; Hayakawa, T. Dry Reforming of Methane over Catalysts Derived from Nickel-Containing Mg-Al Layered Double Hydroxides. *J. Catal.* **2003**, *213*, 191–203.

(16) Shirazi, M.; Neyts, E. C.; Bogaerts, A. DFT Study of Ni-Catalyzed Plasma Dry Reforming of Methane. *Appl. Catal. B Environ.* **2017**, *205*, 605–614.

(17) Kroll, V. C. H.; Swaan, H. M.; Mirodatos, C. Methane Reforming Reaction with

Carbon Dioxide over Ni/$SiO_2$ Catalyst: I. Deactivation Studies. *J. Catal.* **1996**, *161*, 409–422.

(18) Ruckenstein, E.; Hang Hu, Y. Role of Support in $CO_2$ Reforming of $CH_4$ to Syngas over Ni Catalysts. *J. Catal.* **1996**, *162*, 230–238.

(19) Bradford, M. C. J.; Vannice, M. A. $CO_2$ Reforming of $CH_4$ over Supported Pt Catalysts. *J. Catal.* **1998**, *173*, 157–171.

(20) Bradford, M. C. J.; Vannice, M. A. Metal-Support Interactions during the $CO_2$ reforming of $CH_4$ over Model $TiO_x$/Pt Catalysts. *Catal. Letters* **1997**, *48*, 31.

(21) Bitter, J. H.; Hally, W.; Seshan, K.; van, O. J. G.; Lercher, J. A. The Role of the Oxidic Support on the Deactivation of Pt Catalysts during the $CO_2$ Reforming of Methane. *Catal. Today* **1996**, *29*, 349–353.

(22) Nagaoka, K.; Takanabe, K.; Aika, K. I. Modification of Co/$TiO_2$ for Dry Reforming of Methane at 2 MPa by Pt, Ru or Ni. *Appl. Catal. A Gen.* **2004**, *268*, 151–158.

(23) Nagaoka, K.; Okamura, M.; Aika, K. I. Titania Supported Ruthenium as a Coking-Resistant Catalyst for High Pressure Dry Reforming of Methane. *Catal. Commun.* **2001**, *2*, 255–260.

(24) Ferreira-aparicio, P.; Rodr, I. Mechanistic Aspects of the Dry Reforming of Methane over Ruthenium Catalysts. *Appl. Catal.* **2000**, *202*, 183–196.

(25) Huygh, S.; Bogaerts, A.; Neyts, E. C. How Oxygen Vacancies Activate $CO_2$ Dissociation on $TiO_2$ Anatase (001). *J. Phys. Chem. C* **2016**, *120*, 21659–21669.

(26) Sehested, J. Four Challenges for Nickel Steam-Reforming Catalysts. *Catal. Today*, **2006**, *111*, 103–110.

(27) Neyts, E. C.; Ostrikov, K.; Sunkara, M. K.; Bogaerts, A. Plasma Catalysis: Synergistic Effects at the Nanoscale. *Chem. Rev.* **2015**, *115*, 13408–13446.

(28) Neyts, E. C.; Bogaerts, A. Understanding Plasma Catalysis through Modelling and Simulation-a Review. *J. Phys. D. Appl. Phys.* **2014**, *47*, 224010.

(29) Whitehead, J. C. Plasma–catalysis: The Known Knowns, the Known Unknowns and the Unknown Unknowns. *J. Phys. D. Appl. Phys.* **2016**, *49*, 243001.

(30) Bruggeman, P. J.; Czarnetzki, U. Retrospective on "The 2012 Plasma Roadmap." *J. Phys. D. Appl. Phys.* **2016**, *49*, 431001.

(31) Wei, J.; Iglesia, E. Isotopic and Kinetic Assessment of the Mechanism of Reactions of $CH_4$ with $CO_2$ or $H_2O$ to Form Synthesis Gas and Carbon on Nickel Catalysts. *J. Catal.* **2004**, *224*, 370–383.

(32) Snoeckx, R.; Aerts, R.; Tu, X.; Bogaerts, A. Plasma-Based Dry Reforming: A

Computational Study Ranging from the Nanoseconds to Seconds Time Scale. *J. Phys. Chem. C* **2013**, *117*, 4957–4970.

(33) Snoeckx, R.; Setareh, M.; Aerts, R.; Simon, P.; Maghari, A.; Bogaerts, A. Influence of $N_2$ Concentration in a $CH_4/N_2$ Dielectric Barrier Discharge Used for $CH_4$ Conversion into $H_2$. *Int. J. Hydrogen Energy* **2013**, *38*, 16098–16120.

(34) Huygh, S.; Neyts, E. C. Adsorption of C and $CH_x$ Radicals on Anatase (001) and the Influence of Oxygen Vacancies. *J. Phys. Chem. C* **2015**, *119*, 4908–4921.

(35) Snoeckx, R.; Setareh, M.; Aerts, R.; Simon, P.; Maghari, A.; Bogaerts, A. Influence of $N_2$ Concentration in a $CH_4/N_2$ Dielectric Barrier Discharge Used for $CH_4$ Conversion into $H_2$. *Int. J. Hydrogen Energy* **2013**, *38*, 16098–16120.

(36) Kresse, G.; Furthmüller, J. Efficiency of Ab-Initio Total Energy Calculations for Metals and Semiconductors Using a Plane-Wave Basis Set. *Comput. Mater. Sci.* **1996**, *6*, 15–50.

(37) Kresse, G.; Furthmuller, J. Efficient Iterative Schemes for Ab Initio Total-Energy Calculations Using a Plane-Wave Basis Set. *Phys. Rev. B* **1996**, *54*, 11169–11186.

(38) Perdew, J.; Burke, K.; Ernzerhof, M. Generalized Gradient Approximation Made Simple. *Phys. Rev. Lett.* **1996**, *77*, 3865–3868.

(39) Blöchl, P. E. Projector Augmented-Wave Method. *Phys. Rev. B* **1994**, *50*, 17953–17979.

(40) Tkatchenko, A.; Scheffler, M. Accurate Molecular van Der Waals Interactions from Ground-State Electron Density and Free-Atom Reference Data. *Phys. Rev. Lett.* **2009**, *102*, 73005.

(41) Al-Saidi, W. A.; Voora, V. K.; Jordan, K. D. An Assessment of the vdW-TS Method for Extended Systems. *J. Chem. Theory Comput.* **2012**, *8*, 1503–1513.

(42) Ghysels, A.; Verstraelen, T.; Hemelsoet, K.; Waroquier, M.; Van Speybroeck, V. TAMkin: A Versatile Package for Vibrational Analysis and Chemical Kinetics. *J. Chem. Inf. Model.* **2010**, *50*, 1736–1750.

(43) Sheppard, D.; Xiao, P.; Chemelewski, W.; Johnson, D. D.; Henkelman, G. A Generalized Solid-State Nudged Elastic Band Method. *J. Chem. Phys.* **2012**, *136*, 074103.

(44) Sheppard, D.; Henkelman, G. Paths to Which the Nudged Elastic Band Converges. *J. Comput. Chem.* **2011**, *32*, 1769–1771.

(45) Sheppard, D.; Terrell, R.; Henkelman, G. Optimization Methods for Finding Minimum Energy Paths. *J. Chem. Phys.* **2008**, *128*, 134106.

(46) Henkelman, G.; Uberuaga, B. P.; Jónsson, H. Climbing Image Nudged Elastic Band Method for Finding Saddle Points and Minimum Energy Paths. *J. Chem. Phys.* **2000**, *113*, 9901–9904.

(47) Henkelman, G.; Jónsson, H. Improved Tangent Estimate in the Nudged Elastic Band Method for Finding Minimum Energy Paths and Saddle Points. *J. Chem. Phys.* **2000**, *113*, 9978–9985.

(48) Jónsson, H.; Mills, G.; Jacobsen, K. W.; Jonsson, H.; Mills, G.; Jacobsen, K. W. *Classical and Quantum Dynamics in Condensed Phase Simulations*; **1998**; World Scientific, Lerici, 385–404.

(49) Campbell, C. T.; Árnadóttir, L.; Sellers, J. R. V. Kinetic Prefactors of Reactions on Solid Surfaces. *Z. Phys. Chem.* **2013**, *227*, 1435–1454.

(50) Hussain, A.; Gracia, J.; E., N. Ben; Niemantsverdriet, J. W. (Hans). Chemistry of O- and H-Containing Species on the (001) Surface of Anatase $TiO_2$: A DFT Study. *ChemPhysChem* **2010**, *11*, 2375–2382.

(51) Nikolla, E.; Schwank, J.; Linic, S. Promotion of the Long-Term Stability of Reforming Ni Catalysts by Surface Alloying. *J. Catal.* **2007**, *250* (1), 85–93.

(52) Abild-Pedersen, F.; Nørskov, J. K.; Rostrup-Nielsen, J. R.; Sehested, J.; Helveg, S. Mechanisms for Catalytic Carbon Nanofiber Growth Studied by Ab Initio Density Functional Theory Calculations. *Phys. Rev. B* **2006**, *73*, 115419.

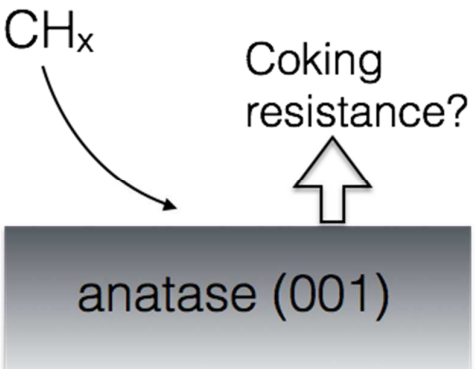


TOC Graphic